Available online at BCREC website: https://bcrec.id

Bulletin of Chemical Reaction Engineering & Catalysis, 14 (3) 2019, 513-520

Research Article

bcl Morphology Formation Strategy on Nanostructured Titania via Alkaline Hydrothermal Treatment

Fry V. Steky[1], Veinardi Suendo[1,2]*, Rino R. Mukti[1,2], Didi P. Benu[1,3], Muhammad Reza[1], Damar R. Adhika[2], Viny V. Tanuwijaya[2], Ashari B. Nugraha[2]

[1]Division of Inorganic and Physical Chemistry, Faculty of Mathematics and Natural Sciences, Institut Teknologi Bandung, Jl. Ganesha No. 10, Bandung 40132 Indonesia
[2]Research Center for Nanosciences and Nanotechnology, Institut Teknologi Bandung, Jl. Ganesha No 10, Bandung 40132, Indonesia
[3]Department of Chemistry, Universitas Timor, Jl. Eltari, Kefamenanu 85613, Indonesia

Received: 7th December 2018; Revised: 27th March 2019; Accepted: 10th April 2019; Available online: 30th September 2019; Published regularly: December 2019

Abstract

Titanium dioxide (TiO_2) is a semiconductor material that plays an important role in photocatalysis. Bi-continuous concentric lamellar (*bcl*) is an interesting morphology with an open channel pore structure that has been successfully synthesized on silica-based materials. If *bcl* morphology can be applied in TiO_2 system, then many surface properties of TiO_2 can be enhanced, i.e. photocatalytic activity. A simple and effective strategy has been demonstrated to transform aggregated and spherical TiO_2 particles to *bcl* morphology via alkaline hydrothermal route. Alkaline hydrothermal treatment successfully transforms TiO_2 particle surface to have *bcl* morphology through swelling with ammonia then followed by phase segregation process. We proposed this strategy as a general pathway to transform the particle surface with any shape to have *bcl* morphology.

Keywords: Alkaline hydrothermal treatment; *bcl* morphology; lamellar morphology; modified morphology; nanostructured TiO_2

How to Cite: Steky, F.V., Suendo, V., Mukti, R.R., Benu, D.P., Reza, M., Adhika, D.R., Tanuwijaya, V.V., Nugraha, A.B. (2019). *bcl* Morphology Formation Strategy on Nanostructured Titania via Alkaline Hydrothermal Treatment. *Bulletin of Chemical Reaction Engineering & Catalysis*, 14(3): 513-520 (doi:10.9767/bcrec.14.3.3853.513-520)

Permalink/DOI: https://doi.org/10.9767/bcrec.14.3.3853.513-520

1. Introduction

Titanium dioxide (TiO_2) is an important inorganic semiconductor material in various applications due to its photosensitive, photostable, and environmentally friendly properties [1]. The advantages properties of TiO_2 provide potential applications in many fields such as photocatalysts [2], dye-sensitized solar cells [3], and catalyst support [4]. Due to its wide application, research about synthesis, characterization and fundamental understanding of TiO_2 material has been intensively studied in last recent years. Many researchers developed TiO_2 synthesis methods to enhance the TiO_2 activity in various applications [5,6], especially as photocatalysts.

Many research groups reported that particle size and morphology are important to obtain TiO_2 with good photocatalytic activity [7-9]. The effective charge transfer in photocatalyst TiO_2 requires the presence of surface active sites [10].

*Corresponding Author.
E-mail: vsuendo@chem.itb.ac.id (V. Suendo)
Phone: +62-22-2502103, Fax: +62-22-2504154

Have a high surface area is the essential requirement to have high surface-active sites photocatalyst. The common strategy to increase surface area is by reducing the crystallite size. However, small TiO_2 particles have low mechanical strength and easily agglomerate to form larger particles. We can use another strategy to increase the surface area of TiO_2 particles by modifying its morphology. Conventional mesoporous TiO_2 has only closed channel pore structure from intercrystallite spaces. However, closed channel pore structure has several drawbacks, such low accessibility due to diffusion limitation, pore blocking, and difficult pore surface activation, despite its high selectivity. Therefore, in vast reaction schemes, the open channel is more favorable. TiO_2 particles with open channel structure provide high surface area, high accessibility and facile pore surface modification [11]. Photocatalytic activity of mesoporous materials with open channel pore structure is easy to adjust chemically due to large reachable surfaces [12].

One of morphology with an open channel pore structure that attracts much attention is bicontinuous concentric lamellar (*bcl*) morphology. *bcl* morphology has been successfully synthesized in various type silica-based materials using reverse micelle templating method [13]. The morphology of *bcl* silica is quite unique. Here, uniform spherical particles consist of bicontinuous lamellae arranged concentrically providing high surface area, large pore volume, and high accessibility [13]. If this morphology can be applied in TiO_2 system, then many surface properties of TiO_2 can be enhanced, i.e. photocatalytic activity. Synthesis of TiO_2 with reverse micelle has been reported elsewhere, but only TiO_2 particles with irregular morphology obtain in the form of aggregates. This type of particles provides low photocatalytic activity [14]. *bcl* morphology cannot be obtained using the reverse micelle templating due to the hydrolysis nature of TiO_2 precursors, i.e. $TiCl_4$, TTIP, etc. It is a rule of thumb that TiO_2 precursors hydrolysis rapidly event in the traces of water.

Herein, we demonstrate the transformation of aggregated and spherical TiO_2 particles to *bcl* morphology via alkaline hydrothermal treatment. Synthesis of nanostructured TiO_2 with *bcl* morphology will be carried out in two simple steps without surfactant. Slow hydrolysis is the main strategy to form TiO_2 particles with controllable particle shape. Swelling and phase segregation is the key to obtain bicontinuous lamellar morphology.

2. Materials and Methods

2.1 Preparation of Nanostructured TiO_2 with *bcl* Morphology

Titanium dioxide was synthesized by modifying previously reported method [5]. First, 1.1 mL of Titanium (IV) isopropoxide (TTIP, 99%, Sigma–Aldrich) was added to 100 mL of ethanol (99%, Merck) under vigorous stirring for 30 minutes until milky white suspension formed. It was kept static for 12 hours and then filtered. The powder obtained was washed with deionized (DI) water and ethanol, and dried at 60 °C for 6 hours. Then, 0.3 g of as-prepared TiO_2 was dissolved in 24 mL of ammonia (25%, Sigma–Aldrich) together with 12 mL of DI water. The mixture was transferred to a 50 mL Teflon-line stainless steel autoclave and heated to 120 °C for 6 hours. After that, the autoclave was cooled down to room temperature naturally. The obtained products were filtered and washed with DI water and ethanol. Finally, the powder obtained was calcined at 500 °C for 1 hour. All the steps above are repeated using the same method with absolute ethanol is replaced by DI water.

Within this study, the samples are designated as TiO_2-A (aggregated as-synthesized), TiO_2-S (spherical as-synthesized), TiO_2-A-HT (aggregated after hydrothermal treatment), TiO_2-S-HT (spherical after hydrothermal treatment), TiO_2-A-HT-500 (aggregated after hydrothermal treatment and calcination at 500 °C), and TiO_2-S-HT-500 (spherical after hydrothermal treatment and calcination at 500 °C).

2.2 Sample Characterizations

The morphology of obtained samples was characterized with scanning electron microscopy (SEM, Hitachi SU3500) with the accelerating voltage at 10 kV. The phase structures were determined by Raman spectroscopy (Bruker – Senterra) with a 532 nm Nd:YAG DPSS (diode-pumped solid-state) laser at 2 mW on 5s scanning time and X-ray diffraction (XRD, Bruker D8 Advance with LynxEye XE detector) on a Scintag diffractometer with CuKα1 radiation (λ = 1.54060 Å) at a scanning rate of 0.239° s^{-1} in the 2θ range from 10 to 90°. Photoluminescence signals were measured by a UV-visible fiber spectrometer (USB4000 Ocean optics) coupled to a 120x magnification microscope objective lens equipped with a 405 nm long-wave pass edge filter (Semrock Edge-Basic, BLP01-405R-25). The sample was excited by a 405 nm diode laser equipped with a 405 nm laser clean-up filter (Semrock MaxLine,

LL01-405-12.5) and a focusing lens setup. N_2 physisorption were carried out using a Quantachrome NOVAtouch LX[4].

3. Results and Discussion

Nanostructured TiO_2 with *bcl* morphology was prepared as explained in the Experimental Section. As shown in Figure 1a and 1b, the aggregate and spherical shape particles were investigated by SEM. The main difference in preparation condition between two kinds of resulted particles is the hydrolysis rate of TiO_2 precursor. TTIP dissolved in DI water experiences rapid hydrolysis, thus produces aggregated particles with an irregular shape. On the other hand, if DI water was replaced by ethanol, TTIP experiences a slow hydrolysis pathway to producing spherical particles.

Figure 1c and 1d show the morphology of particles after alkaline hydrothermal treatment. We observed the surface of both aggregates and spherical particles transform into bicontinuous lamellar morphology. Alkaline hydrothermal treatment has been proved to be independent of particle shape and synthesis history. If the particles have not been calcined yet, then the method can be applied.

Based on results above, we hypothesized that the formation of these lamellar structures was carried out by chemically modifying the surface of particles through swelling and phase segregation under alkaline condition. Figure 1e and 1f show the SEM images of samples after calcination at 500 °C for 6 h. Both images show no significant changes in their morphology after calcination process with respect to Figure 1c and 1d, respectively. Although SEM images do not show noticeable morphology changes after the calcination process, Raman, XRD, and BET analysis reveal significant differences.

Figure 2a shows Raman spectra of synthesized TiO_2 samples. In principle, Raman analysis is not a sensitive method to distinguish particle morphology, i.e. both uncalcined aggregated and spherical particles give relatively similar Raman spectra. However, Raman is very sensitive to distinguish different chemical components and polymorphism in crystalline materials, i.e. between anatase and rutile TiO_2 polymorphs.

In sample TiO_2-A and TiO_2-S shows broad bands at 200, 450, and 610 cm^{-1}. These peaks were frequently observed in amorphous TiO_2 [15]. In sample TiO_2-A-HT and TiO_2-S-HT, the peaks are seen at 190, 270, 440, and 650 cm^{-1}. These peaks due to the formation of titanate species during alkaline hydrothermal process [15]. Moreover, aggregated particles (TiO_2-A-HT) provide spectra with richer features and sharper peaks with respect to spherical particles (TiO_2-S-HT). This might due the aggregated particles have more defects on their surfaces, which is in good agreement with SEM results depicted in Figure 1c and 1d, respectively.

After calcined samples demonstrate typical anatase peaks with Raman shift at 154.50,

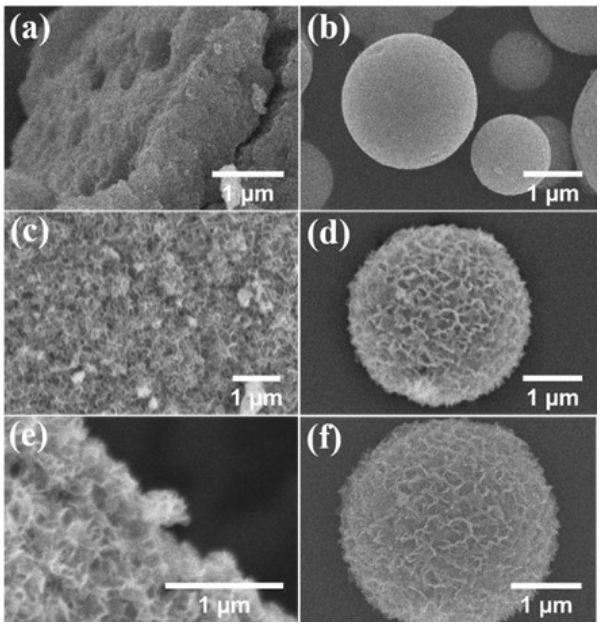

Figure 1. SEM images of nanostructured TiO_2 obtained after different processes: (a) TiO_2-A, (b) TiO_2-S, (c) TiO_2-A-HT, (d) TiO_2-S-HT, (e) TiO_2-A-HT-500 and (f) TiO_2-S-HT-500.

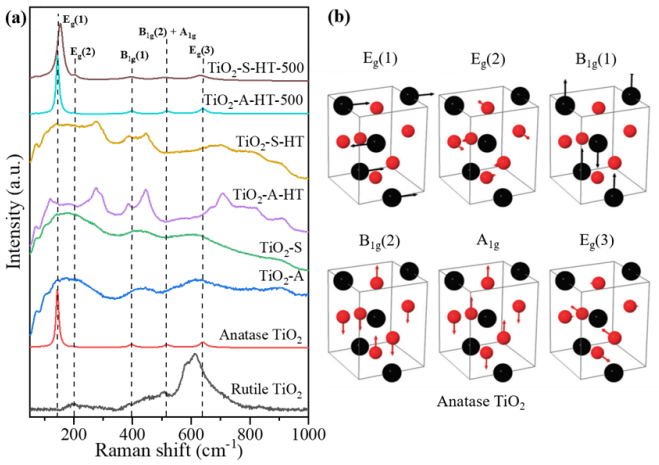

Figure 2. (a) Raman spectra of standard anatase (RRUFF ID: R070582) and rutile (RRUFF ID: R060745), TiO_2-A, TiO_2-S, TiO_2-A-HT, TiO_2-S-HT, TiO_2-A-HT-500, TiO_2-S-HT-500, and (b) schematic of anatase vibrational modes [17].

206.04, 396.18, 513.34, and 631.73 cm^{-1} that assigned to the vibrational modes $E_g(1)$, $E_g(2)$, $B_{1g}(1)$, $B_{1g}(2)+A_{1g}$, and $E_g(3)$, respectively [16]. These peaks represent the vibrational normal modes of anatase as depicted schematically in Figure 2b. Rutile peaks cannot be observed in a calcined sample without deconvolution. In other hands, there are no anatase or rutile peaks can be observed in Raman spectra of uncalcined samples.

To get more structural insights of synthesized TiO_2, XRD analysis must be performed.

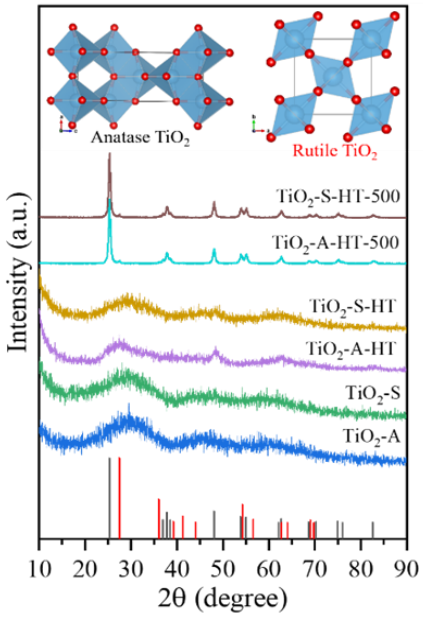

Figure 3. XRD pattern of standard anatase [21] and rutile [22], TiO_2-A, TiO_2-S, TiO_2-A-HT, TiO_2-S-HT, TiO_2-A-HT-500, and TiO_2-S-HT-500 with anatase and rutile structures.

Figure 3 shows the diffractogram of all samples, including the reference standard of rutile and anatase polymorphs. The inset of Figure 3 shows the crystal structure of anatase and rutile. Uncalcined samples (TiO_2-A, TiO_2-S, TiO_2-A-HT, and TiO_2-S-HT) demonstrate similar XRD pattern consists of three broad amorphous peaks at 15.3-35.6°, 42.4-52.3°, and 57.2-70.1° [18-20]. The calcined samples show dominant anatase phase with a trace rutile phase. The peaks at 25.3, 36.9, 37.8, 38.7, 48.0, 53.9, 55.1, 62.1, 62.7, 68.7, 70.3, 75.0, 76.1, and 82.7° are assigned to the anatase phase [21]. A trace peak at 27.48° is assigned to the rutile phase [22].

Based on XRD and Raman analysis results, we propose that the structural precursor of anatase phase obtained after calcination has already resided in all uncalcined samples. The structural precursor feature is more pronounced in XRD than in Raman results, represents by three broad amorphous peaks. Structural precursor appears in Raman spectra only as a broad background. Alkaline hydrothermal treatment does not alter much this feature in XRD pattern, only one additional peak appears around 48.05°, represents the anatase phase. This structural precursor feature can be used to indicate where the calcination process will terminate. In this case, the calcination of this material mainly leads to the formation of the anatase phase.

As shown by Raman and XRD measurements, both of TiO_2-A-HT and TiO_2-S-HT are in amorphous state and turn into anatase crystalline phase after calcination at 500 °C (TiO_2-A-HT-500 and TiO_2-S-HT-500). Amorphous

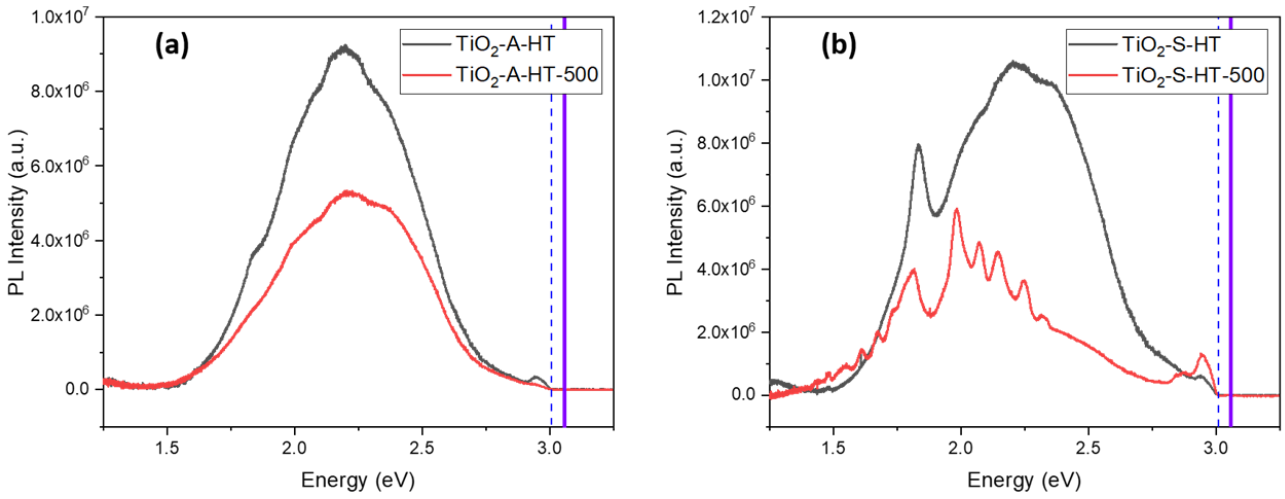

Figure 4. Photoluminescence spectra of synthesized TiO_2 particles before and after calcined process for (a) aggregate and (b) spherical *bcl* particles.

phase in uncalcined samples provide higher defect density, i.e. surface defects, resulting higher photoluminescence (PL) intensity [23-25]. Figure 4 shows PL spectra of synthesized TiO_2 before and after calcination for both aggregate and spherical *bcl* particles. The dash-line is the limit of long wave pass filter and the straight-line represented the excitation laser line at 405 nm. The calcination process transforms amorphous titania phase into anatase crystalline phase decreasing defect density (see Figure 2 and 3). Thus, samples after calcination provide lower PL intensity due to the decrease of defects [23-25]. In TiO_2-S-HT-500 samples, we observed many sharp peaks with ordered spacing around 600 cm^{-1} that corresponds to the phonon coupling of $E_g(3)$ vibrational normal modes of anatase in electronic transition (see Figure 4b) [26].

N_2 physisorption measurements were conducted to characterize surface properties of synthesized particles, i.e. the specific surface areas, pore volume, and pore diameter. The BET and BJH analysis results are presented in Table 1. In general, the specific surface area of the particles increases after alkaline hydrothermal treatment. For spherical particles, this is attributed to the increase of pore volume and the decrease of pore diameter. On the other hand, this is only attributed to the decrease of pore diameter for aggregated particles. This result is in a good agreement with the SEM analysis where alkaline hydrothermal treatment modifies the surface of particles through swelling and phase segregation resulting lamellar morphology with higher surface area (see Figure 1c and 1d). The calcination process decreases the specific surface area of the parti-

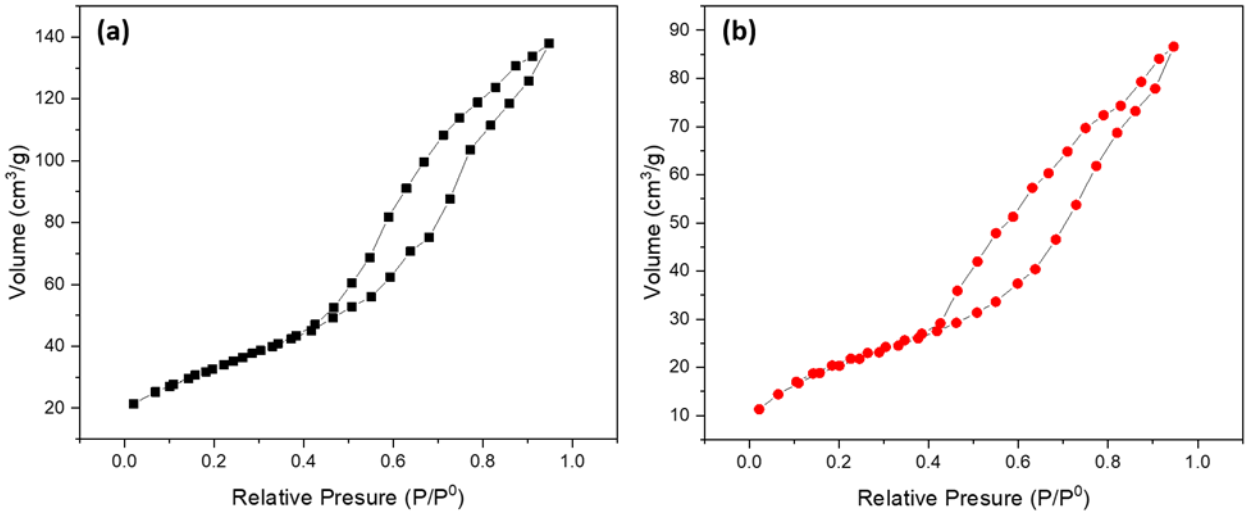

Figure 5. N_2 physisorption isotherm of synthesized TiO_2 particles (a) TiO_2-A-HT-500, and (b) TiO_2-S-HT-500.

Table 1. N_2 Physisorption Analysis Results of Synthesized TiO_2 particles

Sample	Specific surface area $(m^2.g^{-1})^a$	Pore volume $(cm^3.g^{-1})^b$	Pore diameter $(nm)^b$
TiO_2-A	211	0.384	7.25
TiO_2-A-HT	253	0.292	4.62
TiO_2-A-HT-500	119	0.214	7.17
TiO_2-S	82	0.181	17.45
TiO_2-S-HT	337	0.317	7.53
TiO_2-S-HT-500	74	0.134	7.22

[a]) Multi-point BET
[b]) BJH pore size distribution adsorption results

cles. This is mainly due to the decrease of pore volume for spherical particles and the increase of pore diameter for aggregated particles. Figure 5a and 5b show the N_2 physisorption isotherms of TiO_2-A-HT-500 and TiO_2-S-HT-500 samples, respectively. According to Figure 5a and 5b, we suggest the synthesized TiO_2 particles has a type IVa isotherm where capillary condensation is accompanied by hysteresis that starts to occur for pores larger than 4 nm in diameter [27]. In this isotherm, we can also observe the characteristic of type H3 hysteresis loop that occurs due to the presence of the non-rigid aggregates of plate-like particles (i.e. particles with lamellar morphology) but also if the pore network consists of macropores which are not completely filled with pore condensate (i.e. continuous v-groove or open channel networks) [27]. Thus, this type of isotherm supports the presence of *bcl* morphology on the particle surfaces [13].

Although the particles growth mechanism is still obscure, we proposed a general pathway based on *bcl* silica formation mechanism [13] and this result, to transform oxide particle with any shapes to *bcl* morphology (see Figure 6). Here, we demonstrated the transformation of aggregated and spherical TiO_2 particles to *bcl* morphology via alkaline hydrothermal route (see Figure 1c and 1d). This process shows a significant increase in specific surface area, especially for spherical particles. The specific surface area for calcined samples, both aggregated and spherical particles, is still higher with respect to state-of-the-art TiO_2 nanoparticles for photocatalyst, Degussa/Aeroxide P25 (S_{BET} = 35-65 m^2g^{-1}) [28-30], despite of their microscopic size.

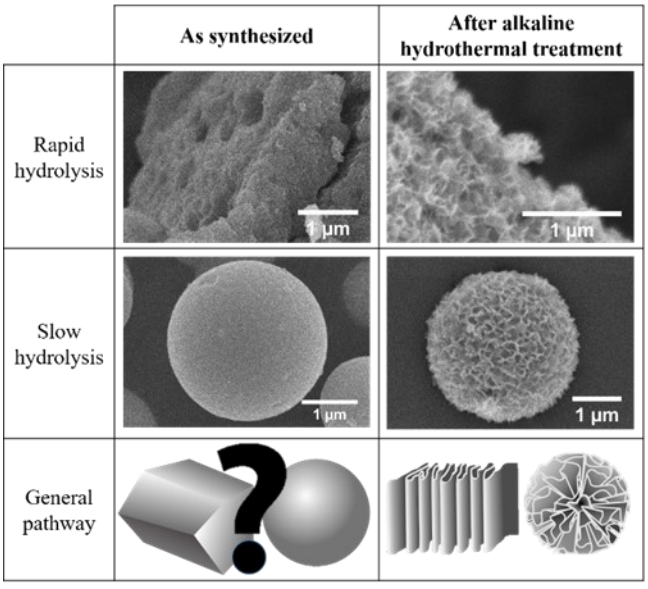

Figure 6. Schematic of TiO_2 synthesis route to produce different particle shape with *bcl* morphology.

4. Conclusions

A simple and effective strategy has been demonstrated to transform aggregated and spherical particles to *bcl* morphology via alkaline hydrothermal route. We proposed this strategy as a general pathway to transform the particle surface with any shape to have *bcl* morphology. This strategy succeeded to achieve TiO_2 particles with a higher specific surface area than the state-of-the-art TiO_2 nanoparticles, Degussa/Aeroxide P25, despite of their microscopic size. This proposed synthesis strategy will open a new perspective in the development of mesoporous materials with open channel pore structure and their applications in a vast variety of fields.

Acknowledgments

This research was financially supported by ITB Research Grant 2018 as a part of ITB Research and Innovation Program 2018. F. V. Steky acknowledges Directorate General of Higher Education for *Bidik Misi* scholarship. Muhammad Reza acknowledges Ministry of Education and Culture of Indonesia for the scholarship through Beasiswa Unggulan. D. P. Benu acknowledges *Lembaga Pengelola Dana Pendidikan* (LPDP) for scholarship support. Authors also acknowledge financial support from Faculty of Mathematics and Natural Sciences, Institut Teknologi Bandung for participation in ICMNS 2018.

References

[1] Yeh, S.W., Ko, H.H., Chiang, H.M., Chen, Y.L., Lee, J.H., Wen, C.M., Wang, M.C. (2014). Characteristics and Properties of a Novel In Situ Method of Synthesizing Mesoporous TiO_2 Nanopowders by a Simple Co-precipitation Process without Adding Surfactant. *Journal of Alloys and Compounds*, 613: 107–116.

[2] Liu, G., Liu, L., Song, J., Liang, J., Luo, Q., Wang, D. (2014). Visible Light Photocatalytic Activity of TiO_2 Nanoparticles Hybridized by Conjugated Derivative of Polybutadiene. *Superlattices and Microstructures*, 69: 164–174.

[3] Latini, A., Cavallo, C., Aldibaja, F.K., Gozzi, D. (2013). Efficiency Improvement of DSSC Photoanode by Scandium Doping of Mesoporous Titania Beads. *J. Phys. Chem. C*, 117: 25276−25289.

[4] Hao, C., Lv, H., Mi, C., Song, Y., Ma, J. (2016). Investigation of Mesoporous Niobium-Doped TiO_2 as an Oxygen Evolution Catalyst Support in an SPE Water Electrolyzer. *ACS Sustainable Chem. Eng.*, 4: 746–756.

[5] Jitputti, J., Rattanavoravipa, T., Chuangchote, S., Pavasupree, S., Suzuki, Y., Yoshikawa, S., Qiu, J. (2009). Fabrication of Size-Controllable Flower-Like TiO_2 and Its Photocatalytic Activity. *Journal of the American Ceramic Society*, 16: 3–9.

[6] Chen, X., Mao, S.S. (2007). Titanium Dioxide Nanomaterials: Synthesis, Properties, Modifications, and Applications. *Chem. Rev.*, 107: 2891-2959.

[7] Lee, J., Orilall, M.C., Warren, S.C., Kamperman, M., DiSalvo, F.J., Wiesner, U. (2008). Direct Access to Thermally Stable and Highly Crystalline Mesoporous Transition-Metal Oxides with Uniform Pores. *Nat. Mater*, 7: 222-228.

[8] Zhou, H.S., Li, D.L., Hibino, M., Honma, I. (2005). A Self-Ordered, Crystalline-Glass, Mesoporous Nanocomposite for Use as A Lithium-Based Storage Device with Both High Power and High Energy Densities. *Angew. Chem. Int. Ed*, 44: 797-802.

[9] Alivov, Y., Fan, Z.Y. (2009). A Method for Fabrication of Pyramid-Shaped TiO_2 Nanoparticles with a High {001} Facet Percentage. *J. Phys. Chem. C.*, 113: 12954–12957.

[10] Nowotny, J., Bak, T., Nowotny, M.K., Sheppard, L.R. (2006). TiO_2 Surface Active Sites for Water Splitting. *J. Phys. Chem. B*, 110: 18492-18495

[11] Bayal, N., Singh, R., Polshettiwar, V. (2017). Nanostructured Silica-Titania Hybrid using Fibrous Nanosilica as Photocatalysts. *ChemSusChem*, 10: 2182-2191.

[12] Dhiman, M., Chalke, B., Polshettiwar, V. (2015). Efficient Synthesis of Monodisperse Metal (Rh, Ru, Pd) Nanoparticles Supported on Fibrous Nanosilica (KCC-1) for Catalysis. *ACS Sustainable Chem. Eng.*, 3: 3224−3230

[13] Febriyanti, E., Suendo, V., Mukti, R.R., Prasetyo, A., Arifin, A.F., Akbar, M.A., Marsih, I.N. (2016). Further Insight on the Definite Morphology and Formation Mechanism of Mesoporous Silica KCC-1. *Langmuir*, 32: 5802-5811.

[14] Inaba, R., Fukahori, T., Hamamoto, M., & Ohno, T. (2006). Synthesis of Nanosized TiO_2 Particles in Reverse Micelle Systems and Their Photocatalytic Activity for Degradation of Toluene in Gas Phase. *Journal of Molecular Catalysis A: Chemical*, 260: 247–254.

[15] Fernández-García, M., Wang, X., Belver, C., Hanson, J.C., Rodriguez, J.A. (2007). Anatase-TiO_2 Nanomaterials: Morphological/Size Dependence of the Crystallization and Phase Behavior Phenomena. *The Journal of Physical Chemistry C*, 111(2): 674–682.

[16] Liu, X-Y., Coville, N.J. (2005). A Raman Study of Titanate Nanotubes. *S. Afr. J. Chem.*, 58: 110–115.

[17] Ohsaka, T., Izumi, F., Fujiki, Y. (1978). Raman Spectrum of Anatase, TiO_2. *Journal of Raman Spectroscopy*, 7(6): 321–324.

[18] Frank, O., Zukalova, M., Laskova, B., Kurti, J., Koltai, J., Kavan, L. (2012). Raman Spectra of Titanium Dioxide (Anatase, Rutile) with Identified Oxygen Isotopes (16, 17, 18). *Phys. Chem. Chem. Phys.*, 14: 14567–14572.

[19] Li, Y., Qin, Z., Guo, H., Yang, H., Zhang, G., Ji, S., Zeng, T. (2014). Low-Temperature Synthesis of Anatase TiO2 Nanoparticles with Tunable Surface Charges for Enhancing Photocatalytic Activity. *PLoS ONE*, 9(12): e114638.

[20] Spada, E.R., Pereira, E.A., Montanhera, M.A., Morais, L.H., Freitas, R.G., Costa, R.G.F., Soares, G.B., Ribeiro, C., de Paula, F.R. (2017). Preparation, Characterization and Application of Phase-Pure Anatase and Rutile TiO_2 Nanoparticles by New Green Route. *Journal of Materials Science: Materials in Electronics*, 28(22): 16932–16938.

[21] Li, Z., Zhu, Y., Wang, J., Guo, Q., Li, J. (2015). Size-Controlled Synthesis of Dispersed Equiaxed Amorphous TiO_2 Nanoparticles. *Ceramics International*, 41(7): 9057–9062.

[22] Rezaee, M., Khoie, S.M.M., Liu, K.H. (2011). The Role of Brookite in Mechanical Activation of Anatase-to-Rutile Transformation of Nanocrystalline TiO_2: An XRD and Raman Spectroscopy Investigation. *CrystEngComm*, 13: 5055–5061.

[23] Howard, C.J., Sabine, T.M., Dickson, F. (1991). Structural and Thermal Parameters for Rutile and Anatase. *Acta Crystallographica, Section B*, 47: 462–468.

[24] Memesa, M., Lenz, S., Emmerling, S.G.J., Nett, S., Perlich, J., Müller-Buschbaum, P., Gutmann, J.S. (2011). Morphology and Photoluminescence Study of Titania Nanoparticles. *Colloid and Polymer Science*, 289(8): 943–953.

[25] Nakajima, H., Mori, T., Watanabe, M. (2004). Relationship between Photoluminescence Intensity of TiO_2 Suspension Containing Ethanol and Its Surface Coverage on TiO_2 Surface. *Japanese Journal of Applied Physics*, 43(6A): 3609–3610.

[26] Zhu, Y.C., Ding, C.X. (1999). Investigation on the Surface State of TiO_2 Ultrafine Particles by Luminescence. *Journal of Solid State Chemistry*, 145(2): 711–715.

[27] Liu, B., Wen, L., Zhao, X. (2007). The Photoluminescence Spectroscopic Study of Anatase TiO_2 Prepared by Magnetron Sputtering. *Materials Chemistry and Physics*, 106(2-3): 350–353.

[28] Thommes, M., Kaneko, K., Neimark, A.V., Olivier, J.P., Rodriguez-Reinoso, F., Rouquerol, J., Sing, K.S.W. (2015). Physisoption of Gases, with Special Reference to the Evaluation of Surface Area and Pore Size Distribution (IUPAC Technical Report). *Pure and Applied Chemistry*, 87(9-10):1–19.

[29] Evonik Resource Efficiency GmbH. (2018, January). AEROXIDE® TiO_2 P25: Hydrophilic Fumed Titanium Dioxide. Product Information. Available at https://products-re.evonik.com/www2/uploads/productfinder/AEROXIDE-TiO2-P-25-EN.pdf (Retrieved March 26, 2019); p. 1.

[30] Schmidt, C. M., Weitz, E., Geiger, F. M. (2006). Interaction of the Indoor Air Pollutant Acetone with Degussa P25 TiO_2 Studied by Chemical Ionization Mass Spectrometry. *Langmuir*, 22(23): 9642–9650.

[31] Suttiponparnit, K., Jiang, J., Sahu, M., Suvachittanont, S., Charinpanitkul, T., Biswas, P. (2011). Role of Surface Area, Primary Particle Size, and Crystal Phase on Titanium Dioxide Nanoparticle Dispersion Properties. *Nanoscale Research Letters*, 6: 27–35